



## Characterization of DC series arc faults in PV systems based on current low frequency spectral analysis

Giovanni Artale<sup>a</sup>, Giuseppe Caravello<sup>a</sup>, Antonio Cataliotti<sup>a</sup>, Valentina Cosentino<sup>a,\*</sup>, Dario Di Cara<sup>b</sup>, Salvatore Guaiana<sup>b</sup>, Nicola Panzavecchia<sup>b</sup>, Giovanni Tinè<sup>b</sup>

<sup>a</sup> Department of Engineering, University of Palermo, Viale delle Scienze, 90128 Palermo, Italy

<sup>b</sup> National Research Council (CNR), Institute of Marine Engineering (INM), Via Ugo La Malfa, 153, 90146 Palermo, Italy

### ARTICLE INFO

#### Keywords:

Arc fault detection  
Electrical safety  
Fault diagnosis  
Series arcs  
PV systems  
UL 1699B

### ABSTRACT

This work presents an experimental study focused on the characterization of series arc faults in direct current (DC) photovoltaic (PV) systems. The aim of the study is to identify some relevant characteristics of arcing current, which can be obtained by means of low frequency spectral analysis of current signal. On field tests have been carried out on a real PV system, in accordance with some tests requirements of UL 1699B Standard for protection devices against PV DC arc faults. Arcing and non-arcing current signals are acquired and compared and the behavior of a set of indicators proposed by authors is analyzed. Different measurement equipment have been used, in order to study the impact of both measurement transducers and data acquisition systems on proposed indicators effectiveness. Presented results show that the considered indicators are suitable for detecting the arc presence even with commercial devices normally used for smart metering applications.

### 1. Introduction

The increasing demand and interest for green energy production has led to a widespread diffusion of distributed generation from renewable energy sources; in this framework photovoltaic (PV) systems play a very important role, with the deployment of PV plants of different sizes, from large “solar farms”, with a high number of panels strings, to small installations for residential and commercial applications. This has caused some safety risks and the need of proper solutions for fault detection and reliability assessment of PV panels, plants and related equipment [1–5].

In this framework a very important issue is the detection of arc faults occurrence [6,7]. Specifically, arc faults are unintentional arcing conditions which may lead to fire ignition, unless they are promptly detected and extinguished by de-energizing the electrical circuit. The arc fault phenomenon can occur in both AC and DC electrical circuits. In PV systems, arc faults events can happen, due to various reasons, such as worn electrical insulation, components aging, stress, overheat or damaged wires and connectors. Arc faults can be basically classified in series arcs and parallel arcs [8]. Series arcs are due to a loss of continuity of a conductor, connection, module or other PV system components,

while parallel arcs occur between two conductors or between a conductor and ground. Typically, series arcs detection is more challenging than parallel arcs detection. In fact, parallel arcs behaves as a sort of short-circuit and they are characterized by levels of current higher than the normal one; on the other hand, in the case of a series arc, the current amount is limited by the load of the PV system components themselves, thus normal and arcing current amplitudes can be very similar. Furthermore, the arc fault phenomenon is intrinsically random and intermittent; during a fault event, normal and arcing current portions can follow each other in the current waveform; the arcing signal can be also filtered, masked or attenuated because of several factors, such as inverter distortion and noise or PV system topology, health and operating conditions, which can modify the arcing signal waveform and characteristics. Due to these reasons, the arcing condition may go undetected or a normal operating condition can be mistaken for an arcing one.

At regulatory level, in order to protect against fire risk due to arcing occurrence, arc-fault circuit interrupters (AFCIs) have been introduced also for PV systems, as previously done for AC applications in dwelling units [9]. Since 2011, the U.S. National Electrical Code (NEC) requires

\* Corresponding author at: Department of Engineering, University of Palermo, Viale delle Scienze, Building. 9, 90128 Palermo, Italy.

E-mail addresses: [giovanni.artale@unipa.it](mailto:giovanni.artale@unipa.it) (G. Artale), [giuseppe.caravello02@unipa.it](mailto:giuseppe.caravello02@unipa.it) (G. Caravello), [antonio.cataliotti@unipa.it](mailto:antonio.cataliotti@unipa.it) (A. Cataliotti), [valentina.cosentino@unipa.it](mailto:valentina.cosentino@unipa.it) (V. Cosentino), [dario.dicara@cnr.it](mailto:dario.dicara@cnr.it) (D. Di Cara), [guaiana.salvatore@inwind.it](mailto:guaiana.salvatore@inwind.it) (S. Guaiana), [nicola.panzavecchia@cnr.it](mailto:nicola.panzavecchia@cnr.it) (N. Panzavecchia), [giovanni.tine@cnr.it](mailto:giovanni.tine@cnr.it) (G. Tinè).

<https://doi.org/10.1016/j.measurement.2021.109770>

Received 29 January 2021; Received in revised form 8 May 2021; Accepted 13 June 2021

Available online 22 June 2021

0263-2241/© 2021 The Authors. Published by Elsevier Ltd. This is an open access article under the CC BY license (<http://creativecommons.org/licenses/by/4.0/>).

that all PV systems with DC circuits operating at 80 V or greater on a building must be protected by AFCIs [10]. The Standard UL 1699B was then introduced in 2012 and further updated on 2018 [11]. It covers requirements for DC PV arc fault circuit protection devices with rated voltage of 1500 V or less. These requirements cover devices including PV AFCIs, arc fault detectors (AFDs), interrupting devices and inverter, converters and charge controllers with integrated arc fault circuit protection. The Standard provides both construction and performance requirements, including arc fault detection tests, “unwanted tripping” tests and related risk analysis, in order to cope with situations in which the AFCI may not trip even if an arc fault is present (trip failure), or it may trip, even when an arc is not present (unwanted trip). On the other hand, the Standard does not provide any specific requirement on the arc fault detection methodology.

As regards the arcing current characteristics, there are some important features in both AC and DC arcs. In AC systems, a typical arcing current is characterized by some distinctive features, such as “shoulders” (i.e. nearly flat zero-current segments in each half cycle, as current extinguishes before and reignites after the normal zero-crossing), high rates of rise and peaks, high-frequency broadband noise (from tens of kilohertz to about 1 GHz), non-stationarity. Such characteristics can be more or less distinguishable, depending on load conditions; for example, in the presence of masking loads, normal current can be very similar to that of an arcing condition and thus arc detection can be more difficult [12]. In comparison with AC phenomenon, a DC arc does not have zero crossing segments, thus it can be more persistent. Broadband noise remains a prominent characteristic of a DC arc (up to about 1 MHz). Typically, due to the inductive behavior of cables, the noise level decreases as frequency increases. As already mentioned, DC arc characteristics can be affected by noisy conditions and disturbances due to the normal operation of the electric system [13–19]. Generally speaking, arc noise and variation depend on a lot of factors, such as electric circuit materials and topologies, voltage and current level, load and supply characteristics. Cables length can act as an antenna, introducing noise in the frequency band of hundreds of kilohertz. Crosstalk effects and power electronic components can introduce harmonics and high frequency noise. Current steps and variations due to load shifting, inverter power adjustment or environmental phenomena (fast moving clouds, wind vibrations, etc.) can determine current waveforms similar to arc faults.

Several papers and patents can be found in literature concerning arc fault detection in AC systems [12], and the research on DC arc faults is ongoing too, concerning both DC arc fault modeling and detection methods [20–31]. More or less realistic arc fault models have been introduced to develop and verify in simulation the arc fault detection methodologies. They can be classified in physics-based models (i.e. based on physical principles), V-I empirical models (i.e. obtained from experimental measurements) and heuristic models (which include additional parameters in the model to better correlate simulation and experimental data). Some of them can be usefully applied for applications on PV arc faults. However, even if such models can be useful for preliminary arc fault detection studies, they have some limitations due to implementation difficulties, validity ranges (in terms of arc type, current level or arc length), as well as for characterization of data acquisition and signal processing techniques, where real measurement issues should be taken into account (such as sampling requirements or computational burden, as well as accuracy features). Thus experimental studies are needed, in order to reproduce real arcing conditions, as well as to test real measurement and protection equipment (as required in [11]). Due to difficulties of modeling the arc condition some new data based or machine learning based techniques were developed. Also the arc fault detection methodology is still a challenging issue and a unique and complete solution, able to correctly operate in all working condition is not yet available.

In this framework the authors have proposed and patented an arc fault detection method [32], based on the measurement of a set of indicators mainly obtained from low frequency spectral analysis of the

current signal. This entails some advantages concerning the constraints on measurement equipment features, in terms of both transducers, data acquisition systems and signal processing requirements. In fact, different problems can arise when measuring typical arcing parameters, such as those in the broadband frequency range; for example, such measurements can require the employment of sophisticated signal processing systems, with high processing speed and/or sampling frequencies, or they can be affected by current transducers and data acquisition systems, which may have a poor frequency response and a low signal-to-noise ratio. On the contrary, by measuring the proposed indicators in the low frequency range, it is possible to reach a good tradeoff between sampling parameters and computational burden, without the need of sophisticated measurement instrumentation. This can also allow the implementation of metrics for arc fault detection in measurement platforms commonly used for smart metering purpose, as well as their integration in commercial equipment installed in PV systems for various monitoring and management purposes (fault detection, efficiency and power quality measurements, field data acquisition, islanding detection and so on) [33–35]. In this perspective, in [36] the authors presented a preliminary study, which showed a qualitative comparison among waveforms and low frequency spectra of DC arcing and non-arcing currents; the comparison results confirmed that low frequency current spectra can be suitably exploited to distinguish the arc fault occurrence from normal operation.

Starting from the preliminary results of [36], this paper presents an extended experimental characterization of the series arcs in DC systems, based on the measurement of the set of indicators proposed in [12]. The aim of the study is to investigate their suitability for DC arcs detection purpose, taking into account also the impact of measurement equipment, i.e. transducers and data acquisition systems, on their effectiveness. In more detail, in [36] a preliminary qualitative comparison was made between normal and arcing current signals and related low frequency spectra. In this paper the experimental characterization is extended, by including the analysis of the behavior of the indicators proposed in [12] for the DC arc phenomenon characterization in the low frequency range. Both laboratory experiments and on-field tests are reported, where arcing and non-arcing current signals are compared and the behavior of the proposed set of indicators is analyzed. On field tests have been carried out on a real PV system, in accordance with some tests requirements of UL 1699B Standard. In all tests, current signals have been acquired with different measurement equipment; in detail, the experimental measurements have been carried out with the following different experimental setup configurations: a high resolution data acquisition board, with both a current shunt and a Hall effect current transducer; a low resolution data acquisition board with both the current shunt and the Hall effect current transducer; a commercial platform for smart metering applications, with embedded transducer and data acquisition. The comparison among the results obtained with different metering equipment allowed verifying the feasibility of using common smart metering platforms even for arc detection purposes.

The paper is organized as follows. Section II presents an overview of DC arcs detection methods. Section III summarizes the UL 1699B requirements for arc detection tests and unwanted tripping tests. The experimental tests and the results obtained are presented and discussed in section IV. The results obtained show that the considered indicators are suitable for detecting the arc presence even when they are measured with commercial devices normally used for smart metering applications.

## 2. DC arc faults detection methods

The research on DC arc faults detection has been recently fostered by the growing interest and protection needs in DC power systems applications such as microgrids, electric vehicles, PV systems. Some arc faults detection methods have been specifically developed for PV systems; other solutions have been proposed for different applications, such as DC microgrids or electric vehicles, but they can be adapted also for PV arcs

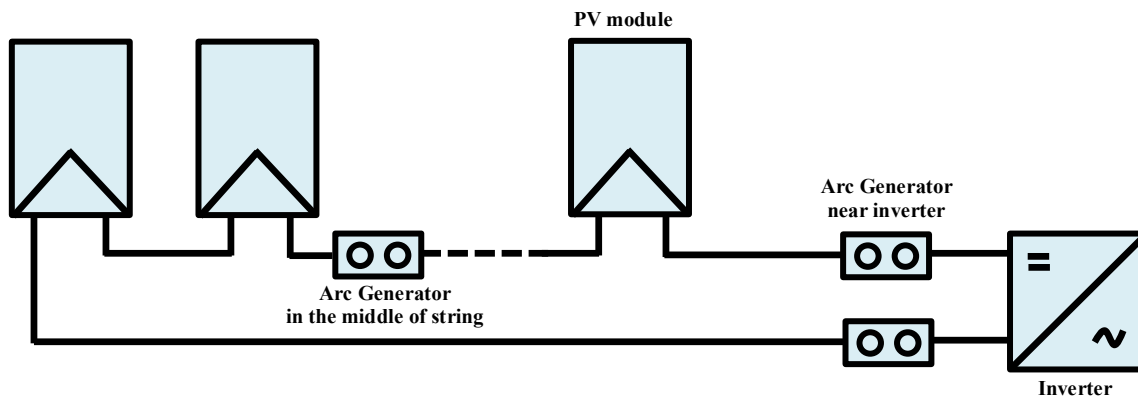


Fig. 1. Scheme of UL1699B use case for arc detection tests. Use case of One string, one MPPT.

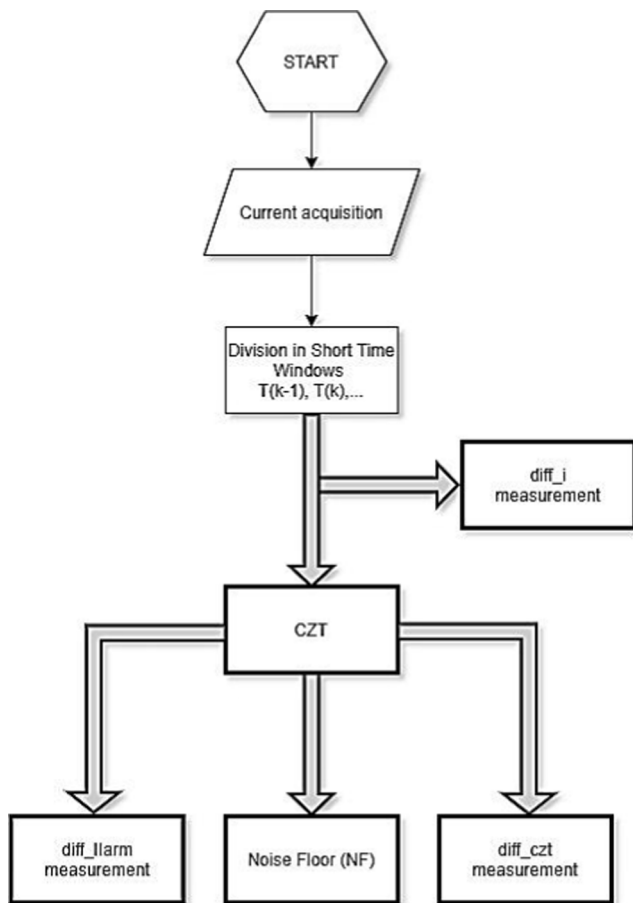


Fig. 2. Arc Fault analysis flowchart.

recognition [19–24]. Most methods are based on current (and, less frequently, voltage) signal analysis, in both frequency and time domain.

In the frequency domain, one of the most studied signal characteristics is the broadband noise (typically from tens of kilohertz up to 100 kHz). Some studies make a specific analysis of frequency components within the aforesaid bands; for example in [31] frequency components from 5 to 40 kHz are investigated, by means of a “circuit modeling” test setup, configured as those of UL1699B (i.e. test circuit setup for PV system emulation). Fast Fourier Transform (FFT) is generally used to evaluate amplitude and/or power of signal spectrum in specified frequency bands; measured values are compared with given thresholds to discriminate between normal and arcing conditions. In this viewpoint,

when predetermined thresholds are used, some limitations can arise with respect to methods robustness in real operating conditions, where arc characteristics can vary depending on noisy conditions, inverter operation and so on. To improve detection accuracy, the use of adaptive thresholds has been proposed, which are statistically determined from the analysis of the signal in subsequent observation windows; in these cases a problem to cope with is related signal changes during the normal operation of the system (for example start-up or power changes). As regards the measurement equipment and signal processing requirements, broadband spectral analysis poses some issues concerning sampling parameters choice, observation window, frequency resolution and reasonable computational burden and complexity. In fact, for the implementation of the aforesaid methods, required sampling frequencies and number of acquired samples are relatively high, if compared with the typical sampling and memory features of commercial platforms typically used for power systems measurements applications.

Methods based on time domain and statistical analysis can allow lower sampling frequencies and computational costs. In such methods, RMS, magnitude or peak values of the current/voltage signal are measured for the arc detection purpose. To individuate distinctive high and random variations of arcing conditions, signal rate of change or difference of maximum and minimum value are monitored and compared with given thresholds. Statistical analysis, proper estimators and outlier analysis are proposed to evaluate the variance of the signal and to determine anomalies with respect to V-I characteristics which can be related to an arc fault occurrence. As for frequency domain analysis, main limitations of such approaches are related to threshold values used for distinguishing arcing from normal operating conditions and to noise and disturbances introduced by PV system equipment which can affect the arc detection capability.

Some “multi criteria” methods have been also proposed to improve the arc detection accuracy; in such methods both time and frequency domain characteristics are simultaneously monitored (for example time domain fluctuations and specific frequency components spikes). Some solutions make use of Short Time Fourier Transform (STFT) analysis, where the trend is analyzed of the considered frequency components over time. In other cases, methods based on Discrete Wavelet Transform (DWT) or Wavelet Packet Decomposition (WPD) have been proposed to improve signal analysis resolution into the frequency bands of interest. Further methods are based on Artificial intelligence (AI) techniques, such as artificial neural network (ANN), support vector machine (SVM) or other machine learning techniques; In [28] an innovative algorithm for detecting L-L faults in PV arrays based on support vector machine (SVM) was proposed. However this approach was not tested in a series arc fault condition and also has the drawback of needing a large amount of data. The authors in [29] try to mitigate this drawback with the use of graph-based semi-supervised learning models. Generally speaking, for most aforesaid methods, main problems still remain concerning high

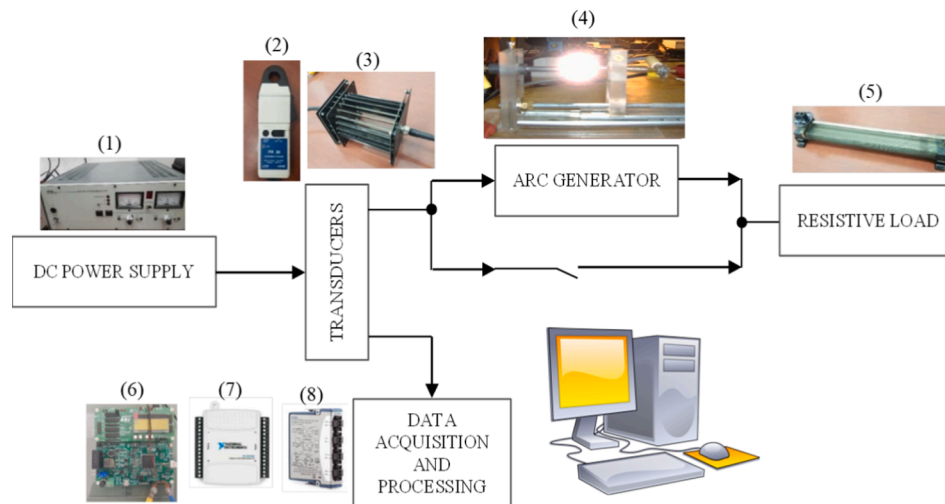


Fig. 3. Scheme of the laboratory test bench.

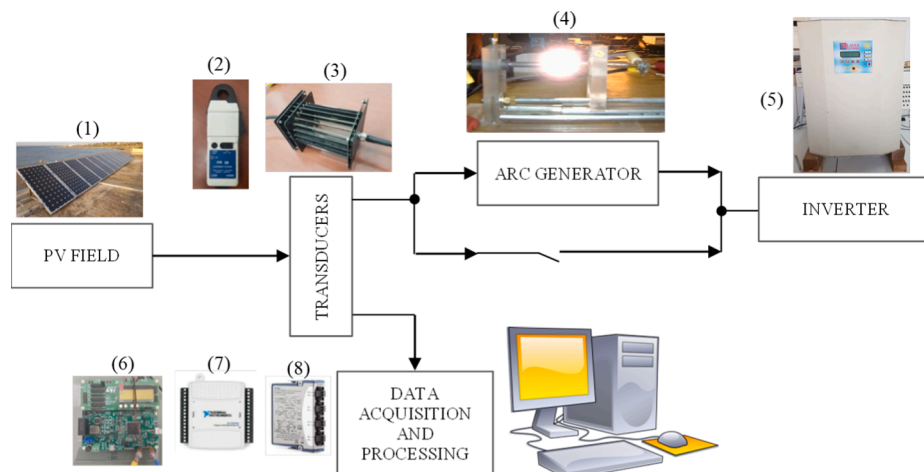


Fig. 4. Scheme of the on-field test bench.

computational burden, complexity and reliability.

Only few methods for fault detection in PV systems make use of signal analysis in low frequency range (up to few kilohertz or lower). This is mainly due to the fact that environmental noise due to PV power electronics may overlap with low frequency components of the arc signals, and this can potentially affect the detection methods based on such signatures. However, as observed in [36], the possibility of exploiting low frequency analysis can allow reducing sampling requirements and computational burden, thus enabling the use of commercial acquisition and signal processing systems which typically have low sampling frequency and limited memory and computational capabilities. In this framework, the choice of sampling frequency and number of acquired samples is crucial to obtain a good tradeoff between spectral resolution and the observation window. In fact, typical processing algorithms for frequency-domain analysis (such as FFT) are known to require the signal stationarity in the observation window. On the other hand, arc signal, in both AC and DC systems, is typically non stationary, thus the observation window should be as small as possible, in order to maintain valid the condition of stationary signal. This can cause a poor spectral resolution. Thus, the algorithm used for the frequency analysis should be able to ensure a good spectral resolution even with very short observation windows. Furthermore, when dealing with the measurement chain, attention should be paid to the measurement transducers, whose behavior can be critical when high frequency components must be

acquired and processed. The possibility to use low frequency analysis can allow to better face all the aforesaid problems.

### 3. UL 1699B. Arc fault detection tests and unwanted tripping tests

As already mentioned, the Standard UL 1699B [11] provide construction and performance requirements of DC arc fault circuit protection devices, which are intended for use in PV electrical energy systems. The arc fault detector (AFD) provide protection from the risk of fire ignition due to arcing occurrence, by detecting the fault and enabling the power interruption.

Requirements regarding the constructions of the different parts of the protection devices cover various aspects, such as corrosion resistance, internal wiring, type of insulation, type of power supply, operating mechanisms, programmable electronic components, safety requirements for operation under power. As regards the devices performance, several tests are required, in order to verify the correct devices functioning. Tests are specified under varying environmental conditions (temperature, humidity, corrosion, electromagnetic and power quality disturbances) and in presence of leakage currents, overvoltages, insulation tests, mechanical tests. Arc fault detection tests and unwanted tripping tests are also considered to test the capability of correctly detecting the arcing conditions and distinguish them from normal

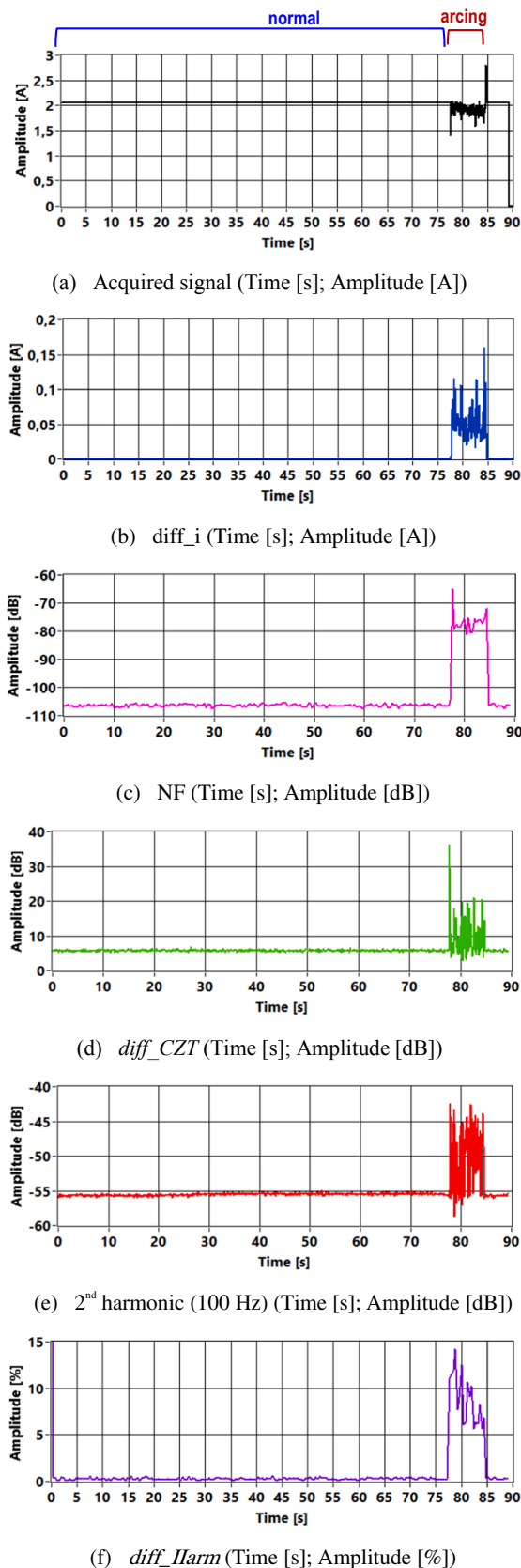


Fig. 5. Laboratory test with NI9239 and current shunt. Acquired current and measured indicators.

operating conditions, even when noise or other disturbances may occur.

As regards arc fault detection tests, the UL 1699B [11] defines the various application cases in which the device under test (DUT) must be tested, including the circuit requirements for the applicable use cases. For example Fig. 1 depicts the scheme for tests in the use case of one string PV and one Maximum Power Point Tracker (MPPT), where the different positions of the arc generator used for tests are highlighted. Other configuration tests involve the presence of two strings combined and one MPPT. In this case the arc generator can be positioned near the inverter or between two strings. If a combiner is involved in PV plant, the arc generator can be positioned near inverter or between two strings. Instead, if DC-DC converters are involved, the arc generator shall be inserted near the converter or in the end of the string. If more input module are connected to a DC-DC converter, arc generator shall be inserted between two strings connected to the converter. In case of microinverter, the arc generator shall be connected between panel and inverter.

The Standard [11] provides also guidelines for the construction of the arc generator. In summary, the arc generator electrodes, one moveable and one stationary, shall be cylindrical, with 6,35 mm diameter, and made of solid copper or tungsten alloy; the electrode mating surfaces shall be parallel, flat, and vertical.

The test procedure for series connection arcing test is also defined in [11], with specific requirements for the arc generator positioning and movements, sequence and number of tests to be performed, arcing tests conditions, voltage and current recording, DUT detection time. In summary, for each test the arc generator must be placed in one of the considered positions; at the beginning of the test the arc generator electrodes are in contact with each other and then they are separated to create the arcing condition. The DUT must detect the arc within the specified intervention time.

A section of [11] is dedicated to the unwanted tripping tests, i.e. tests where particular operating conditions are reproduced where the DUT shall not trip. Different loading conditions are described, which cover the following situations: different inverters, converters and charge controllers (in both single-phase and three-phase cases); DC switch operation; irradiance step changes. For every loading condition, test circuits include one string and two strings configurations and the use of a DC/DC converter with one or two input modules.

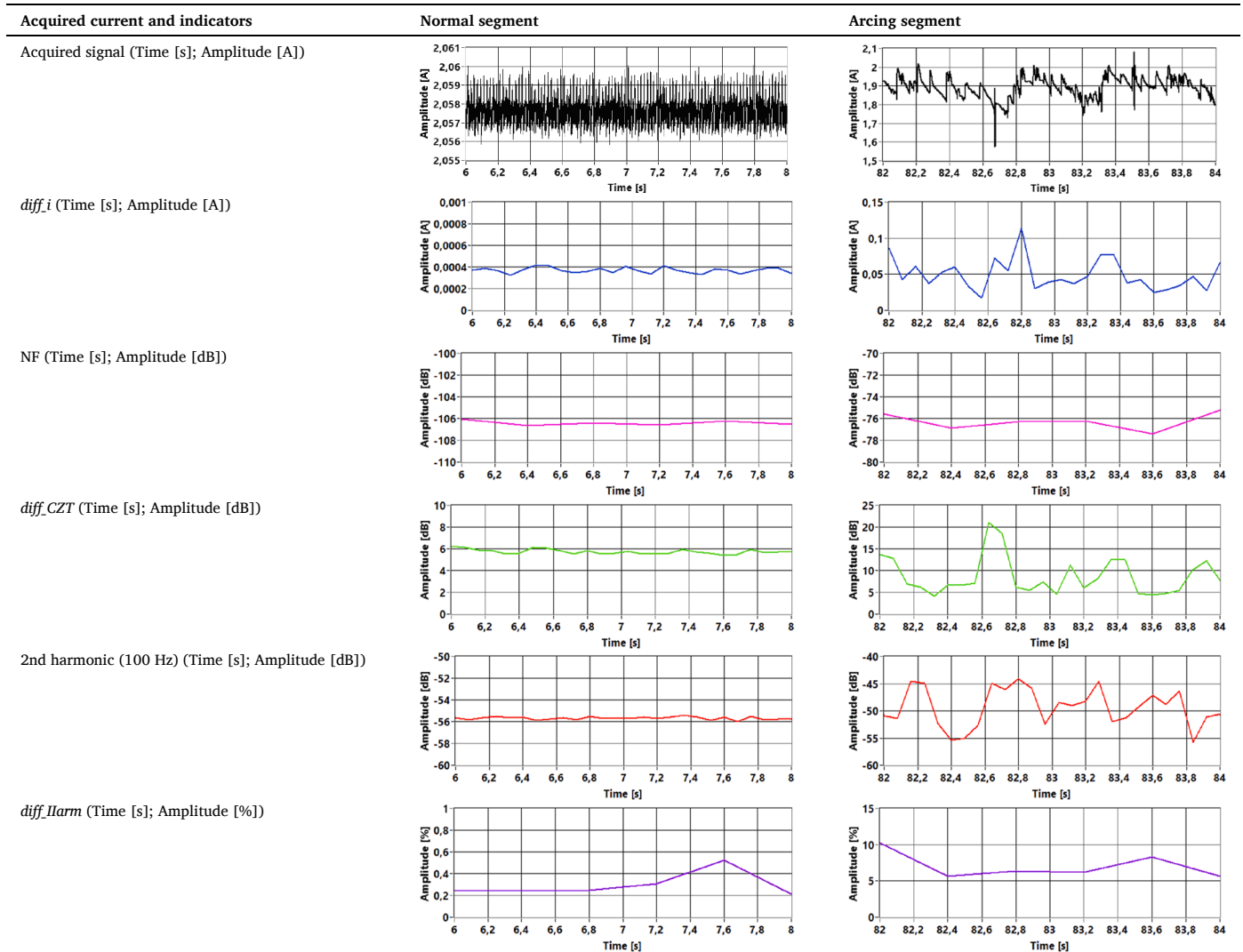
The DUT should be tested for each use case as applicable. To emulate the on-field operating conditions of a real PV plant, the UL1699B provide electrical circuits schemes values for building suitable test setups. They include full details for DC source, decoupling network and half/full string model (module and line impedance), with specified values for all circuit components, according to the different use cases. For example, in the use case of Fig. 1, two DC sources, decoupling networks and half string circuits are considered, in order to allow reproducing both tests with arc generator near to inverter or in middle of the string.

With respect to the aforesaid requirements, in the experimental study presented in this paper, both laboratory and on-field tests were carried out. Laboratory tests were carried out on a simplified test setup with a DC source, a simple resistive load and the arc generator connected between them. This was made in order to make a preliminary characterization of the measurement setup and to investigate the behavior of the considered indicators (previously defined for the AC case) for DC arc faults detection in a simple case study; the simplified test bench allowed investigating the impact of measurement equipment features on the indicators effectiveness, without considering the influence of PV systems components and the inverter, which can introduce further noise and distortion on current waveform. On the other hand, to verify the feasibility of the proposed indicators for PV DC arc faults detection, the on-field tests were carried out on a real PV plant, according to the UL1699B use case of Fig. 1.



**Table 1**

Laboratory test with NI9239 and current shunt. Acquired current and measured indicators. Comparison between normal and arcing segments.

**Table 2**

Laboratory test with NI9239 and current shunt. Measured indicators. Comparison between normal and arcing conditions. Mean values and standard deviations of measured indicators.

Indicator	Normal/arcingcondition	Mean value	Standarddeviation
$diff_i$	Normal	0.004 A	0.001 A
	Arcing	0.05 A	0.02 A
NF	Normal	-106.4 dB	0.5 dB
	Arcing	-77 dB	2 dB
$diff_{czt}$	Normal	5.8 dB	0.2 dB
	Arcing	9 dB	4 dB
II harmonic	Normal	-55.5 dB	0.2 dB
	Arcing	-50 dB	4 dB
$diff_{IIarm}$	Normal	0.3%	0.1%
	Arcing	9%	2%

#### 4. Experimental tests and results

The experimental characterization has been carried out with the aim of investigating the feasibility of low frequency spectral analysis of current for DC arc faults occurrence detection. More in detail, the study has been focused on the behavior of the indicators originally proposed

by the authors in [12] for the AC case, in order to verify their suitability for the distinguishing between arcing and non-arcing condition also in DC case. Furthermore, during the tests, the current signal were acquired by using different transducers and data acquisition devices, in order to analyze to what extent such equipment can affect the measurement of the considered indicators and their effectiveness for the arc fault detection purpose. Experimental tests have been carried out both in laboratory and on-field, by reproducing both non-arcing and arcing conditions, in order to compare the current waveforms and low frequency spectra and the indicators behavior in both the absence and presence of the faulty condition. The following subsections describe the measured indicators, the test bench and metering equipment, the preliminary laboratory characterization and the on-field tests.

##### 4.1. Proposed arc fault detection indicators

In detail, in [12] the authors proposed an arc-fault detection strategy for AC systems, based on the measurement of a set of indicators mainly derived from low frequency spectral analysis of current; to allow obtaining a good resolution even with short observation windows, the chirp zeta transform (CZT) algorithm was chosen to measure the considered indicators. In this paper the indicators proposed in [12] have been evaluated in the case of DC arcs, in order to investigate their effectiveness in the DC case. In detail, the following four indicators

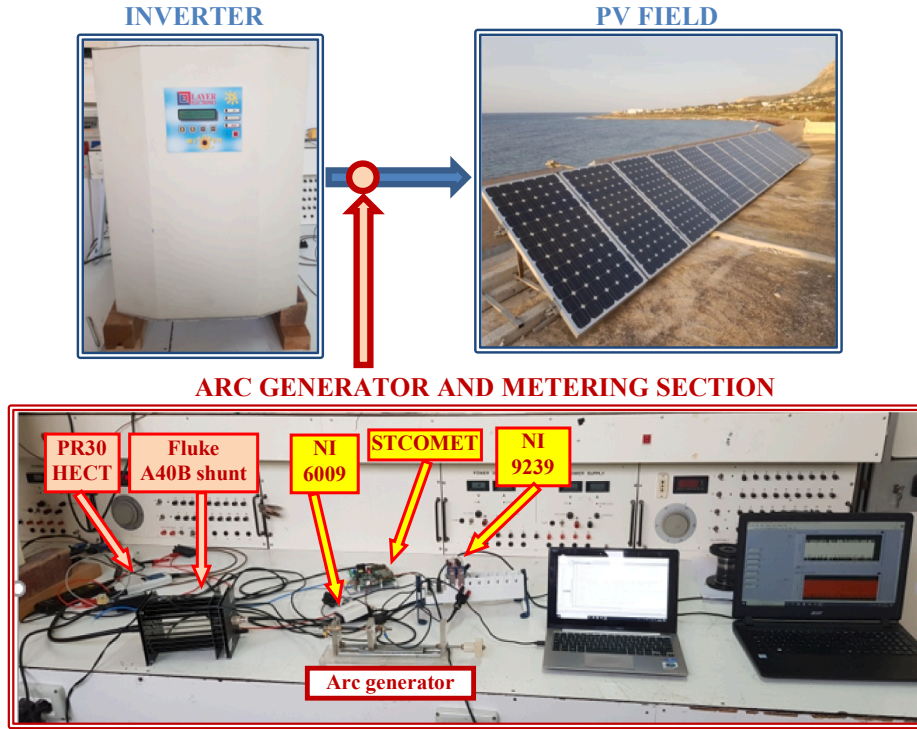


Fig. 6. On-field test bench.

defined in [12] have been considered:

1.  $diff\_czt$ , i.e. the mean value of the differences between the  $N$  samples ( $S_n$ ) of two low-frequency amplitude spectra of the current, measured in two successive observation windows ( $T(k)$  and  $T(k-1)$ ); it is given by

$$diff\_czt = \frac{1}{N} \sum_{n=0}^{N-1} |S_{nT(k)} - S_{nT(k-1)}| \quad (1)$$

2.  $diff\_IIarm$ , i.e. the relative value of the difference between the maximum values of spectra samples  $S_n$  in the frequency interval  $[f2\_min; f2\_max]$ , around the second harmonic (of the fundamental power system frequency), measured in two subsequent observation windows,  $T(k)$  and  $T(k-1)$ ; it is given by:

$$diff\_IIarm = \frac{\left| \max[S_{T(k)}]_{(f2\_min}^{f2\_max)} - \max[S_{T(k-1)}]_{(f2\_min}^{f2\_max)} \right|}{\max[S_{T(k-1)}]_{(f2\_min}^{f2\_max)}} \cdot 100 \quad (2)$$

3.  $NF$ , i.e. the noise floor, evaluated as the mean value of the  $N'$  samples of residual current spectrum  $S'_{T(k)}$ , which is obtained by removing the samples of both odd and even harmonics main lobes from the current spectrum  $S_{T(k)}$ ; it is given by:

$$NF = \frac{1}{N'} \sum_{n \in N'} S'_{nT(k)} \quad (3)$$

4.  $diff\_i$ , i.e. the mean value of the difference between the  $N$  samples of current ( $i_n$ ) acquired in two subsequent observation windows,  $T(k)$  and  $T(k-1)$ ; it is given by

$$diff\_i = \frac{1}{N} \sum_{n=0}^{N-1} |i_{nT(k)} - i_{nT(k-1)}| \quad (4)$$

In previous formulas:

- $S_{T(k)}$  is amplitude spectrum of the current  $i_{T(k)}$  acquired in the observation window  $T(k)$ ;
- $N$  is the number of samples of  $S_{T(k)}$ ;
- $S_{nT(k)}$  and  $S_{nT(k-1)}$  are the  $n$ -th sample of the spectra  $S_{T(k)}$  and  $S_{T(k-1)}$ , measured in the observation windows  $T(k)$  and  $T(k-1)$ , respectively;
- $f2\_max$  and  $f2\_min$ , is the frequency interval corresponding to the main lobe of the second harmonic of the current spectrum  $S$ ;
- $\max[S_{T(k)}]_{(f2\_min}^{f2\_max)}$  is the maximum value of  $S_{T(k)}$  in the specified frequency interval  $[f2\_min; f2\_max]$ ;
- $\max[S_{T(k-1)}]_{(f2\_min}^{f2\_max)}$  is the maximum value of  $S_{T(k-1)}$  in the specified frequency interval  $[f2\_min; f2\_max]$ ;
- $S'_{T(k)}$  is residual amplitude spectrum of the current  $i_{T(k)}$  acquired in the observation window  $T(k)$ , which is obtained by removing the samples of main lobes of both odd and even harmonics from the current spectrum  $S_{T(k)}$ ;
- $N'$  is the number of samples of  $S'_{T(k)}$ ;
- $i_{nT(k)}$  and  $i_{nT(k-1)}$  are the  $n$ -th sample of the currents  $i_{T(k)}$  and  $i_{T(k-1)}$ , measured in the observation windows  $T(k)$  and  $T(k-1)$ , respectively.

As detailed in [12],  $diff\_czt$  and  $diff\_i$  indicators are representative of the signal non-stationarity; in fact, if the signal is stationary, they assume a very small value (ideally zero); on the other hand, if signal is non-stationary, the indicators values increase.  $NF$  is one of the most significant parameters for arc recognition; in fact, it typically increases in arc presence. This was shown in literature with respect to broadband noise in the range of tens/hundreds of kilohertz; in this paper the noise floor and the harmonic components behavior is investigated in the low frequency range (up to few kilohertz), instead. Finally,  $diff\_IIarm$  is an indicator of the trend of second harmonic (of the power system fundamental frequency); as shown in the following, in the study herein presented this indicator has been considered because during the experimental on-field tests it was observed that the acquired current signal was affected by harmonics even in non-arcing conditions; in detail a ripple at 100 Hz was observed, i.e. twice the fundamental power line frequency of 50 Hz (because of the inverter switching) [36].

**Table 3**  
On-field test with NI9239 and current shunt and PR30. Acquired current and measured indicators.

Acquired current and indicators	NI9239 with current shunt	NI9239 with HECT
Acquired signal (Time [s]; Amplitude [A])		
$diff_i$ (Time [s]; Amplitude [A])		
NF (Time [s]; Amplitude [dB])		
$diff_{czt}$ (Time [s]; Amplitude [dB])		
2nd harmonic (100 Hz) (Time [s]; Amplitude [dB])		
$diff_{Iarm}$ (Time [s]; Amplitude [%])		

In Fig. 2 the algorithm flowchart is shown. Current is acquired and for each observation window  $T(k)$  the indicators (1)–(4) are evaluated. The length of the observation window is set in order to have a good resolution for CZT spectral analysis, even with short time windows; in the results presented in this paper, the observation window was set equal to 80 ms (as made in [12]). For each observation window,  $diff_i$  is evaluated starting from current samples, i.e. in the time domain, according to (4). The other indicators are evaluated in the frequency domain, from the current spectrum obtained with the CZT algorithm.

In detail, the measurement of the frequency domain indicators, i.e.  $diff_{czt}$ ,  $diff_{Iarm}$  and  $NF$ , is made starting from a low frequency spectral analysis, in a frequency band up to few kHz. Most existing methods are focused on frequency components in higher frequency bands (tens or even hundreds of kilohertz), instead. However, the possibility of using low frequency spectral analysis allows using low sampling frequencies, such as those commonly used in commercial smart metering equipment (for example in the experimental tests herein presented, values up to 10 kHz were used), with the advantages of reaching a suitable trade-off

between sampling frequency, observation window length, memory requirements, computational burden and cost effectiveness.

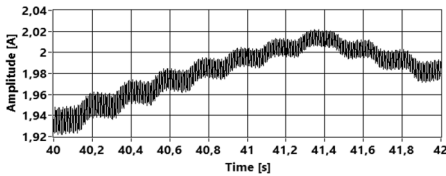
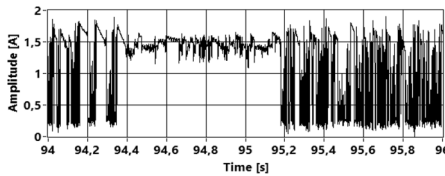
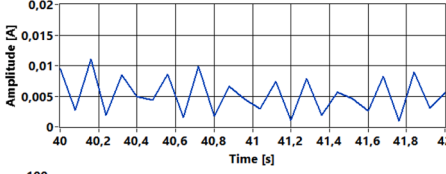
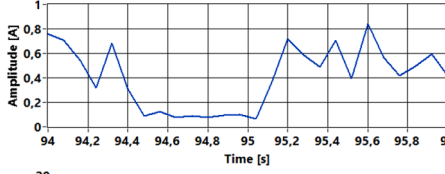
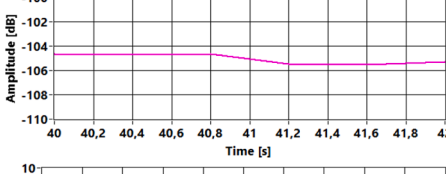
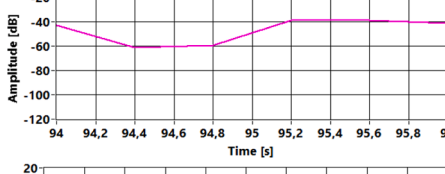
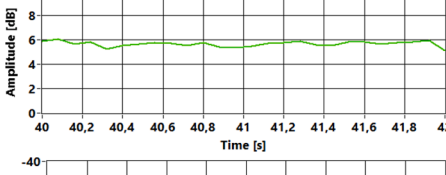
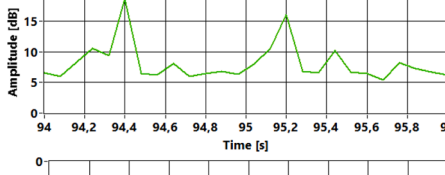
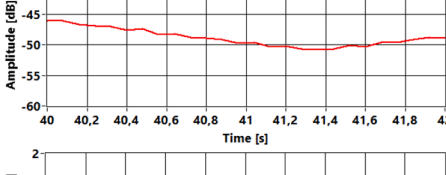
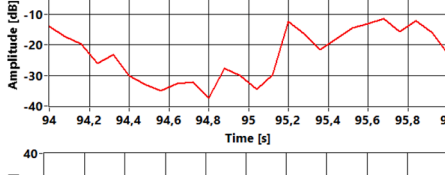
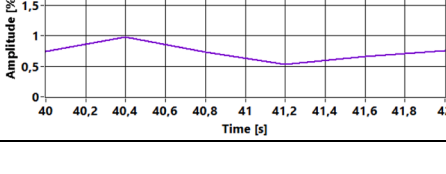
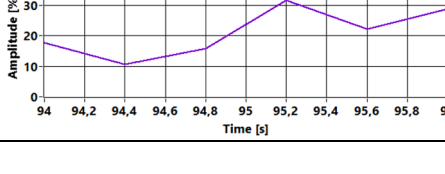
#### 4.2. Test bench and measurement equipment

Experimental measurements were carried out both in laboratory and on-field, on a real PV power plant. The test benches for laboratory and on-field tests are schematized in Fig. 3 and Fig. 4, respectively. In summary, the test bench equipment for laboratory measurements (Fig. 3) were the following: (1) DC Power supply; (2) Hall effect current clamp-on transducer (HECT); (3) Current Shunt; (4) Arc generator; (5) Resistive Load; (6) STCOMET board; (7) NI-DAQ NI6009; (8) NI-DAQ NI9239. Current signals were acquired and processed by PC. As shown in Fig. 4, for on-field tests the arc generator and the metering section were between the PV field (1) and the inverter (5), in according to the scheme of Fig. 1 (arc generator near inverter [36]). The arc generator was built according to UL1699B [11]. During both laboratory and on-field tests, the arc generator was inserted or short-circuited, in order



Table 4

On-field test with ni9239 and current shunt. Acquired current and measured indicators. Comparison between normal and arcing segments.

Acquired current and indicators	Normal segment	Arcing segment
Acquired signal (Time [s]; Amplitude [A])		
$diff_i$ (Time [s]; Amplitude [A])		
NF (Time [s]; Amplitude [dB])		
$diff_{czt}$ (Time [s]; Amplitude [dB])		
2nd harmonic (100 Hz) (Time [s]; Amplitude [dB])		
$diff_{Iarm}$ (Time [s]; Amplitude [%])		

to reproduce both normal (non-arcing) and arcing conditions.

Two types of current transducers and two data acquisition boards were used to sense and acquire the signal. Their main features are listed below.

- Current Shunt: Fluke A40B, maximum current 5 A, nominal resistance 0.16  $\Omega$ , accuracy  $\pm 21 \mu\text{A/A DC}$ ,  $\pm 71 \mu\text{A/A}$  up to 100 kHz (95% confidence level).
- Hall effect current clamp-on transducer (HECT): LEM PR 30, maximum current 20 A, instrument constant 100 mV/A, frequency range from DC to 100 kHz, accuracy  $\pm (1\% \text{ rdg} + 2 \text{ mA})$ , resolution 1 mA.
- NI-DAQ NI9239: four analog voltage differential input channels, simultaneous sampling, input range  $\pm 10 \text{ V}$ , maximum sampling frequency 50kS/s (10 kS/s was used in the tests herein presented), 24-bit ADC delta-sigma with analog anti-aliasing prefiltering, alias-free bandwidth 0.453 of sampling frequency, offset 0.008% of range, gain 0.03% of reading, THD – 99 dB, noise 70  $\mu\text{V}$ .
- NI-DAQ NI6009: multifunction I/O device, four analog voltage differential input channels (eight in single-ended mode), multiplexed, input range from  $\pm 1 \text{ V}$  to  $\pm 20 \text{ V}$ , maximum sampling frequency 48 kS/s (10 kS/s was used in the tests herein presented), 14 bit ADC, absolute accuracy at full scale up to 14.7 mV, noise 0.5 mVrms for  $\pm 1 \text{ V}$  input range and 5 mVrms for  $\pm 20 \text{ V}$  input range).

The measurement of considered indicators was implemented in LabVIEW environment.

The measurements were carried out also with a further device, i.e. an EVLKSTCOMET10-1 by STMicroelectronics (named STCOMET in the following). It is a development kit for smart metering applications, based on STCOMET chip, which integrates both a modem for power line communication (PLC) and a metrology section. Main features of the metrology section are: nominal voltage 230 V, nominal current 5 A, sampling frequency 7.8125 kHz, –3 dB bandwidth 0–3.6 kHz, 24-bit ADC delta-sigma. As regards voltage and current transducers, the STCOMET board includes a resistive divider used as voltage sensor, while both a shunt and a current transformer are available for measuring current; the shunt was used in the experimental tests.

Thus, for each test, measurements were carried out with the following metering equipment configurations:

- NI-DAQ NI9239 with current shunt;
- NI-DAQ NI9239 with HECT;
- NI-DAQ NI6009 with current shunt;
- NI-DAQ NI6009 with HECT;
- STCOMET with embedded current shunt.

In this way it has been possible to investigate not only the indicators feasibility for arc fault detection, but also the impact of both transducers

**Table 5** On-field test with various metering equipment. Measured indicators. Comparison between normal and arcing conditions. Mean values (and standard deviations) for current segments of Table 4.

Indicator	Normal/arcgcondition	NI 9239 with current shunt	NI 9239 with HECT	NI 6009 with current shunt	NI 6009 with HECT	NI 6009 with current shunt	NI 6009 with HECT	STCOMETwith internal current shunt
<i>diff<sub>i</sub></i>	Normal	0.005 A (0.003 A)	0.006 A	0.022 A (0.004 A)	0.024 A	0.025 A		0.025 A
	Arcing	0.40 A (0.25 A)	0.41 A	0.45 A (0.25 A)	0.45 A	0.45 A		0.45 A
<i>NF</i>	Normal	-105 dB (1 dB)	-104 dB	-78 dB (1 dB)	-75 dB	-72 dB		-72 dB
	Arcing	-47 dB (10 dB)	-48 dB	-44 dB (8 dB)	-45 dB	-50 dB		-50 dB
<i>diff<sub>czt</sub></i>	Normal	5.7 dB (0.2 dB)	5.9 dB	5.5 dB (0.2 dB)	5.5 dB	5.3 dB		5.3 dB
	Arcing	8 dB (2 dB)	11 dB	10 dB (2 dB)	10 dB	10 dB		10 dB
<i>II harmonic</i>	Normal	-48 dB (2 dB)	-47 dB	-49 dB (3 dB)	-47 dB	-47 dB		-47 dB
	Arcing	-23 dB (8 dB)	-24 dB	-25 dB (7 dB)	-22 dB	-26 dB		-26 dB
<i>diff<sub>Iharm</sub></i>	Normal	0.7% (0.1%)	0.5%	5% (2%)	5%	7%		7%
	Arcing	20% (8%)	19%	21% (8%)	22%	23%		23%

and data acquisition equipment on their measurement and effectiveness.

### 4.3. Laboratory results

In laboratory tests a DC power supply (Elind mod 500KL) and a 20 Ω/100 W resistor were used for power generation and load, respectively. This allowed measuring the indicators and characterizing the data acquisition systems in a sort of ideal condition, without any disturbance or noise typical of real operating conditions (such as PV inverter noise or current variations). The arc generator was connected in series with the load, in order to reproduce series arcs conditions. During the tests, the arc generator was inserted or short circuited, in order to have both arcing and non-arcing conditions.

As an example, Fig. 5 shows the plots of the acquired current and the indicators of eq. (1)-(4) during a laboratory test with NI-DAQ NI9239 and current shunt. In the current plot of Fig. 5 (a), the normal (without arc) and arcing portions are highlighted. The plots of Fig. 5 (b)-(f) show that all indicators values are essentially constant during the normal operation, while they assume higher values and variability in the presence of arc. In Table 1, segments of normal and arcing current and related indicators are compared. Table 2 shows mean values and standard deviations of the measured indicators, for both normal and arcing segments of the current. It can be observed that the indicators variations from normal to arcing condition are significant thus they can be potentially used for arc detection purpose. Furthermore, in almost all cases, the amount of the indicators variations are higher than the related standard deviations. The best behavior is observed for NF; in fact a variation of about 30 dB is observed from normal to arcing condition, while the standard deviation of the measured values is not higher than 2 dB.

Similar plots, measured values and standard deviations were obtained with the NI-USB 6009 and STCOMET. This suggests the possibility to use also them for arc detecting purposes, even if the lower ADC resolution of NI-USB 6009 and the STCOMET conditioning circuit can significantly affect the indicator absolute values. For example, for noise floor, in normal conditions (DC power supply and no arc), differences of about 25–30 dB were observed between NI9239 *NF* measurements and those of the other devices. These phenomena have been observed also during on-field tests and they will be further explained in next subsection.

### 4.4. On-field results

On field tests were carried out in a 2 kW PV plant installed at the industrial site of Layer Electronics Srl (Erice, Italy). The on-field test bench built at Layer Electronics is shown in Fig. 6. The arc generator and the metering section were placed near the inverter, according to the use case of Fig. 1. The current was simultaneously acquired with all metering equipment configurations previously described, i.e. NI-DAQ NI9239 and NI-DAQ NI6009 with both current shunt HECT and STCOMET with embedded current shunt. Acquired signals were stored and processed by means of two laptops (one for managing data from NI-DAQ boards, the other one for managing data from STCOMET board).

Table 3 shows some results obtained with the NI 9239 board and the two current transducers (Current shunt and HECT). By comparing the plots of acquired current and measured indicators, it can be observed that results are quite similar, thus the transducers does not impact significantly the indicators measurement.

Table 4 shows a comparison between two segments of normal and arcing current and related indicators. It can be seen that the current plot is very noisy and it has a high variability, even in normal condition, due to inverter noise and variations on PV panels solar irradiance. However even in these on field tests, the indicators assume lower and almost constant values during the normal operation, while they have higher values and variability in the presence of arc. The indicators variations from normal to arcing condition are always significant, thus confirming

their effectiveness for arc detection purpose. The worst behavior is observed for the indicator *diff.IIarm*, due to the inverter ripple. As for the laboratory tests, similar plots and variation rates were obtained with the other measurement devices (NI 6009 and STCOMET).

Table 5 shows the comparison between mean values and standard deviations of the indicators measured with the different metering equipment configuration listed in section IV.B (NI-DAQ NI9239 with current shunt; NI-DAQ NI9239 with HECT; NI-DAQ NI6009 with current shunt; NI-DAQ NI6009 with HECT; STCOMET with embedded current shunt). The results are related to the normal and arcing current segments of Table 4. It can be seen that the indicators measured with the different metering equipment have slightly different values; this happens even in normal conditions (and it is more visible for noise floor), due to the differences among the metrological features of employed instrumentation (particularly the data acquisition boards and the STCOMET). However, in all cases the indicators variation between normal and arcing conditions are higher than the variation due to the metering equipment features or time variability of operating conditions. Standard deviations are small if compared with the differences between the indicators values in normal and arcing conditions. Thus the indicators obtained with low frequency analysis of the current signal can allow to achieve reliable information on arc occurrence, even with common equipment for smart metering applications or low-cost data acquisition boards, such as STCOMET or NI-USB 6009.

Furthermore, the on-field results are consistent with those obtained in laboratory, where noise and distortion due to real PV systems components and the inverter were not present. This confirms the feasibility of the proposed indicators for arc faults detection in PV systems, even in the presence of noise, distortion and non-stationary currents due to PV plant normal operation. For example, in the on-field tests, the current waveform in normal conditions was not stationary and distorted, showing a second harmonic (100 Hz) ripple, due to the operation of the inverter; however, this did not affect the feasibility of the proposed indicators.

## 5. Conclusions

This paper has presented an experimental study on DC series arc faults in PV systems using a set of parameters derived from low frequency spectral analysis of current signal. The indicators used for this study were previously proposed by the authors for AC arc fault detection. The experimental characterization herein presented has been aimed at verifying both the indicators suitability for the DC case and the impact of different transducers and data acquisition systems on their measurement and effectiveness.

Both laboratory and on-field tests on a real PV system have been carried out; the experimental setup has been built in accordance with tests requirements of UL 1699B Standard for protection devices against PV DC arc faults. Arcing and non-arc current signals are acquired and compared verifying the behavior of each proposed indicators.

Preliminary laboratory tests allowed comparing the different metering equipment (data acquisition boards and a commercial platform for smart metering applications) in stationary conditions and in non-arc conditions; the results put in evidence the different performances of the equipment under test, in terms of noise and distortion due to ADCs and/or on-board signal conditioning. The same test in the presence of arcs gave a first positive feedback about the use of the proposed indicators also for the DC case.

On field tests allowed investigating the behavior of the considered indicators in a more realistic case, where, even in the absence of arcing, the current signal is not stationary, due to inverter noise or operating conditions variations. According to UL 1699B such conditions can create problems in discriminating normal operation from arc faults occurrence. Tests have been carried out in both arcing and non-arc conditions by using different transducers and data acquisition systems. The obtained results showed that: the employed transducers (current shunts and

HECT) do not affect significantly the indicators measurement; the data acquisition equipment can have a higher impact on the measured values but the proposed indicators in any cases allow detecting arc faults occurrence, even with in the noisy and non-stationary conditions of the real case.

In conclusion, presented results show that the considered indicators are suitable for detecting the arc presence even with commercial devices normally used for smart metering applications. In this viewpoint, the possibility of using low frequency analysis can allow reaching a good tradeoff between sampling parameters and computational burden. This can make feasible the use of low cost commercial platforms for power system measurements, with low sampling frequencies and limited computational and memory capabilities. This could also allow the implementation and integration of arc fault detection algorithms in measurement devices commonly installed at both AC and DC side of PV systems for various monitoring and management purposes, where low frequency spectral analysis can be suitable (fault detection, efficiency and power quality measurements, field data acquisition, islanding detection and so on).

## CRediT authorship contribution statement

**Giovanni Artale:** Software, Data curation, Formal analysis, Investigation, Writing - original draft. **Giuseppe Caravello:** Data curation, Formal analysis, Investigation, Visualization, Writing - original draft. **Antonio Cataliotti:** Conceptualization, Methodology, Validation, Funding acquisition, Project administration. **Valentina Cosentino:** Conceptualization, Methodology, Software, Validation, Writing - review & editing, Supervision. **Dario Di Cara:** Conceptualization, Methodology, Software, Validation, Writing - review & editing, Supervision. **Salvatore Guaiana:** Software, Data curation, Formal analysis, Investigation, Visualization. **Nicola Panzavecchia:** Software, Data curation, Formal analysis, Investigation, Visualization. **Giovanni Tinè:** Conceptualization, Methodology, Validation, Funding acquisition, Project administration.

## Declaration of Competing Interest

The authors declare that they have no known competing financial interests or personal relationships that could have appeared to influence the work reported in this paper.

## Acknowledgment

The research received the financial support of the European Union in the following grants:

- PO FESR Sicilia 2014-2020, Action 1.1.5, Project n. 08000PA90246, Project title: "Smart grids per le isole minori (Smart grids for small islands)", acronym: I-Sole CUP G99J18000540007;
- Program IEV CT Italie Tunisie 2014-2020, Project n. IS\_2.1\_131, Project title: "Solutions innovantes pour l'intégration des énergies renouvelables sur le réseau électrique tunisien", Project acronym: SInERT, CUP: B74I19001040006 and B74I18014130002.

The paper content is responsibility of the authors and it does not necessarily reflect the point of view of the European Union.

The authors would like to thank Layer Electronics Srl for the assistance during on-field tests and the availability of the test site.

## Appendix A. Supplementary data

Supplementary data to this article can be found online at <https://doi.org/10.1016/j.measurement.2021.109770>.

## References

- [1] A.Y. Appiah, X. Zhang, B.B.K. Ayawli, F. Kyeremeh, Review and performance evaluation of photovoltaic array fault detection and diagnosis techniques, *Int. J. Photoenergy* 2019 (2019) 1–19.
- [2] Syafaruddin, D.S. Zinger, Review on methods of fault diagnosis in photovoltaic system applications, *J. Eng. Sci. Technol. Rev.* 12 (5) (2019) 53–66.
- [3] K.-H. Chao, C.-T. Chen, A remote supervision fault diagnosis meter for photovoltaic power generation systems, *Measure.: J. Int. Measure. Confederation* 104 (2017) 93–104.
- [4] L. Cristaldi, M. Faifer, M. Lazzaroni, M.M.A.F. Khalil, M. Catelani, L. Ciani, Diagnostic architecture: a procedure based on the analysis of the failure causes applied to photovoltaic plants, *Measure.: J. Int. Measure. Confederation* 67 (2015) 99–107.
- [5] D.S. Pillai, N. Rajasekar, A comprehensive review on protection challenges and fault diagnosis in PV systems, *Renew. Sustain. Energy Rev.* 91 (2018) 18–40.
- [6] K. Klement, DC arc flash studies for solar photovoltaic systems: challenges and recommendations, *IEEE Trans. Ind. Appl.* 51 (5) (2015) 4239–4244.
- [7] Z. Wu, Y. Hu, J.X. Wen, F. Zhou, X. Ye, A Review for Solar Panel Fire Accident Prevention in Large-Scale PV Applications, *IEEE Access* 8 (2020) 132466–132480.
- [8] J. Yuventi, DC electric arc-flash hazard-risk evaluations for photovoltaic systems, *IEEE Trans. Power Deliv.* 29 (1) (2014) 161–167.
- [9] K.M. Armijo, J. Johnson, R.K. Harrison, K.E. Thomas, M. Hibbs, A. Fresquez, Quantifying photovoltaic fire danger reduction with arc-fault circuit interrupters, *Prog. Photovoltaics Res. Appl.* 24 (4) (2016) 507–516.
- [10] National Electrical Code, NFPA70, National Fire Protection Association, Quincy, MA.
- [11] UL 1699B, Photovoltaic (PV) DC Arc-Fault Circuit Protection, Underwriters Laboratories Inc., 2018.
- [12] G. Artale, A. Cataliotti, V. Cosentino, D. Di Cara, S. Nuccio, G. Tine, Arc fault detection method based on CZT low-frequency harmonic current analysis, *IEEE Trans. Instrum. Meas.* 66 (5) (2017) 888–896.
- [13] Q. Xiong, X. Feng, A.L. Gattozzi, X. Liu, L. Zheng, L. Zhu, S. Ji, R.E. Hebner, Series arc fault detection and localization in DC distribution system, *IEEE Trans. Instrum. Meas.* 69 (1) (2020) 122–134.
- [14] K. AbdulMawjood, S.S. Refaat, W.G. Morsi, Detection and prediction of faults in photovoltaic arrays: A review, 2018 IEEE 12th International Conference on Compatibility, in: *Power Electronics and Power Engineering (CPE-POWERENG 2018)*, Doha, 2018, pp. 1–8.
- [15] Z. Zhang, Q. Chen, R. Xie, K. Sun, The fault analysis of PV cable fault in DC microgrids, *IEEE Trans. Energy Convers.* 34 (1) (2019) 486–496.
- [16] G. Crotti, A. Delle Femine, D. Gallo, D. Giordano, C. Landi, M. Luiso, A. Mariscotti, P.E. Roccatto, Pantograph-to-OHL arc: conducted effects in DC railway supply system, *IEEE Trans. Instrum. Meas.* 68 (10) (2019) 3861–3870.
- [17] A. Delle Femine, D. Gallo, D. Giordano, C. Landi, M. Luiso, D. Signorino, Power quality assessment in railway traction supply systems, *IEEE Trans. Instrum. Meas.* 69 (5) (2020) 2355–2366.
- [18] D. Giordano, D. Signorino, C. Landi, A. Delle Femine, M. Luiso, G. Crotti, Power quality in DC railway system: a facility to characterize the on-board detection systems, in: *24th IMEKO TC4 International Symposium and 22nd International Workshop on ADC and DAC Modelling and Testing*, 2020, pp. 112–116.
- [19] R.F. Ammerman, T. Gammon, P.K. Sen, J.P. Nelson, DC-arc models and incident-energy calculations, *IEEE Trans. Ind. Appl.* 46 (5) (2010) 1810–1819.
- [20] S. Lu, B.T. Phung, D. Zhang, A comprehensive review on DC arc faults and their diagnosis methods in photovoltaic systems, *Renew. Sustain. Energy Rev.* 89 (2018) 88–98.
- [21] M. Ahmadi, H. Samet, T. Ghanbari, Series arc fault detection in photovoltaic systems based on signal-to-noise ratio characteristics using cross-correlation function, *IEEE Trans. Ind. Inf.* 16 (5) (2020) 3198–3209.
- [22] W. Fenz, S. Thumfart, R. Yatchak, H. Roitner, B. Hofer, Detection of arc faults in PV systems using compressed sensing, *IEEE J. Photovoltaics* 10 (2) (2020) 676–684.
- [23] W. Miao, X. Liu, K.H. Lam, P.W.T. Pong, Arc-faults detection in pv systems by measuring pink noise with magnetic sensors, *IEEE Trans. Magn.* 55 (7) (2019) 1–6.
- [24] S. Liu, L. Dong, X. Liao, X. Cao, X. Wang, B.o. Wang, Application of the variational mode decomposition-based time and time-frequency domain analysis on series DC arc fault detection of photovoltaic arrays, *IEEE Access* 7 (2019) 126177–126190.
- [25] S. Lu, T. Sirojan, B.T. Phung, D. Zhang, E. Ambikairajah, DA-DCGAN: an effective methodology for DC series arc fault diagnosis in photovoltaic systems, *IEEE Access* 7 (2019) 45831–45840.
- [26] Z. Wang, R.S. Balog, Arc fault and flash signal analysis in DC distribution systems using wavelet transformation, *IEEE Trans. Smart Grid* 6 (4) (2015) 1955–1963.
- [27] T. Andrianajaina, E.J.R. Sambatra, C. Bernard Andrianirina, T. David Razafimahafoa, N. Heraud, PV fault detection using the least squares method, in: *2016 International Conference and Exposition on Electrical and Power Engineering (EPE)*, Iasi, 2016, pp. 846–851.
- [28] Y. Zhehan, A.H. Etemadi, A novel detection algorithm for Line-to-Line faults in Photovoltaic (PV) arrays based on support vector machine (SVM), in: *2016 IEEE Power and Energy Society General Meeting (PESGM)*, Boston, MA, 2016, pp. 1–4.
- [29] Y. Zhao, R. Ball, J. Mosesian, J. de Palma, B. Lehman, Graph-based semi-supervised learning for fault detection and classification in solar photovoltaic arrays, *IEEE Trans. Power Electron.* 30 (5) (2015) 2848–2858.
- [30] M. Weerasekara, M. Vilathgamuwa, Y. Mishra, Detection of high impedance faults in PV systems using mathematical morphology, in: *2018 IEEE International Conference on Industrial Electronics for Sustainable Energy Systems (IESES)*, Hamilton, 2018, pp. 357–361.
- [31] J.-C. Kim, S.-S. Kwak, Frequency-domain characteristics of series DC arcs in photovoltaic systems with voltage-source inverters, *Appl. Sci.*, 10(22), 8042, pp. 1–14, 2020.
- [32] G. Artale, A. Cataliotti, V. Cosentino, G. Privitera, Arc fault detection equipment and method using low frequency harmonic current analysis, US Patent US9025287; Assignee: STMicronics, 2015.
- [33] N. Erraissi, M. Raoufi, N. Aarich, M. Akhsassi, A. Bennouna, Implementation of a low-cost data acquisition system for PROPRE.MA project, *Measure.: J. Int. Measure. Confederation* 117 (2018) 21–40.
- [34] R.I.S. Pereira, I.M. Dupont, P.C.M. Carvalho, S.C.S. Jucá, IoT embedded linux system based on Raspberry Pi applied to real-time cloud monitoring of a decentralized photovoltaic plant, *Measure.: J. Int. Measure. Confederation* 114 (2018) 286–297.
- [35] A. Reatti, M.K. Kazimierczuk, M. Catelani, L. Ciani, Monitoring and field data acquisition system for hybrid static concentrator plant, *Measure.: J. Int. Measure. Confederation* 98 (2017) 384–392.
- [36] G. Artale, G. Caravello, A. Cataliotti, V. Cosentino, D. Di Cara, S. Guaiana, N. Panzavecchia, G. Tinè, DC series arc faults in PV systems. Detection methods and experimental characterization, in: *24th IMEKO TC4 International Symposium and 22nd International Workshop on ADC and DAC Modelling and Testing*, IMEKO TC-4 2020, 2020, pp. 135–140.